metals

MDPI

Article

Analysis of Temperature and Stress Fields in the Process of Hot-Rolled Strip Coiling

Meng Dai [1,2], Yuting Hu [1,2], Yanchao Hao [1,2], Ping Qiu [2,*] and Hong Xiao [1,2,*]

[1] National Engineering Research Center for Equipment and Technology of Cold Strip Rolling, Yanshan University, Qinhuangdao 066004, China; dai199509@stumail.ysu.edu.cn (M.D.); hyt88571@163.com (Y.H.); haoyanchao@stumail.ysu.edu.cn (Y.H.)
[2] School of Mechanical Engineering, Yanshan University, Qinhuangdao 066004, China
* Correspondence: qiuping@ysu.edu.cn (P.Q.); xhh@ysu.edu.cn (H.X.)

Abstract: During the coiling process of a hot-rolled strip, with the increasing layers the temperature and stress distribution inside the coil constantly change and interact with each other. Due to the contact with the sleeve and the transition of the heat exchange state, it is inaccurate to consider the temperature of the whole coil as the coiling temperature set by the process requirement. Meanwhile, due to the periodic interlayer contact in the radial direction, the relation between stress and deformation is nonlinear. For the coiling process, it is difficult to consider the above factors using conventional methods. Therefore, an incremental model has been established to couple the temperature and stress of the coil. In order to obtain the mechanical properties of the strip and radial elastic modulus of the coil, tensile tests and laminated compression experiments are conducted at different temperatures. The effects of changes in strip thickness, coiling tension, and initial temperature of the sleeve on the stress and the temperature inside the coil are studied. Finally, by comparing the model results with measurements and analytical solutions, the effectiveness of the incremental coupled model is verified and the errors caused by the analytical method are analyzed.

Keywords: hot-rolled strip coiling; stress field analysis; temperature field analysis; incremental method

Academic Editor: Zbigniew Pater

Received: 20 December 2024
Revised: 18 January 2025
Accepted: 20 January 2025
Published: 24 January 2025

Citation: Dai, M.; Hu, Y.; Hao, Y.; Qiu, P.; Xiao, H. Analysis of Temperature and Stress Fields in the Process of Hot-Rolled Strip Coiling. *Metals* **2025**, *15*, 111. https://doi.org/10.3390/met15020111

1. Introduction

As the final process of the hot-rolling production line, coiling directly affects the quality of products [1–3]. The coiling temperature mainly depends on the control of the microstructure and properties of the coil [4–7]. However, there is a significant temperature difference between the cooled strip and the sleeve, resulting in severe heat transfer at the contact position. The temperature drop near the inner ring of the coil can cause changes in the microstructure. During repeated heating and cooling processes, surface cracks and other forms of failure may appear on the sleeve. The defects in the coil are determined by the internal stress state. Excessive tension can lead to defects such as interlayer bonding, deformation of the sleeve, and interlayer slip damage, while insufficient tension can lead to collapse after unwinding [8–10]. Therefore, understanding the temperature and stress distribution inside the coil can provide a theoretical basis to optimize process parameters and reduce defects. Therefore, it is important to establish a model to calculate temperature and stress during the coiling process.

The coil is composed of repeated periodic contact interface layers, and the heat transfer state is significantly different from that of the strip itself [11]. In previous studies, for the

anisotropy caused by interlayer contact, the effective thermal conductivity in the radial direction was commonly used [12–14]. Considering strip thickness, surface characteristics and contact pressure, Park, S.J. [15] established a unit thermal resistance model. Based on this model, Park, S.J. conducted a finite element simulation to analyze the effects of different sizes and cooling methods on the cooling process of the coil. Park, S.J.'s model has been widely applied in research. The thermal resistance model was adopted by Yang, Y.J. [16] to perform differential calculations on the temperature inside the coil, and the thermal deformation during the cooling process was analyzed. Saboonchi, A. [17,18] established a temperature field model for coils stored in the warehouse, and the effects of different stacking methods were discussed. In Cheng, J.F.'s works [19], material density and thickness were considered as the factors affecting thermal conductivity, and the effects of different element compositions of the strip on the temperature field were studied. Witek, S. [20] established a temperature–stress coupled model during the cooling process and analyzed the residual stress distribution after cooling. The above models all focus on the cooling process, and the coiling temperature is considered as the starting point of the cooling process. In fact, due to the heat loss at the axial end faces and the heat exchange between the coil and sleeve, the overall temperature of the coil after coiling is no longer uniform and there is a certain gap with the coiling temperature. Therefore, when using the above thermal resistance model, the real-time changes in the radial thermal conductivity caused by the stress as well as the heat transfer between the coil and the sleeve should be considered. For solving the above problems, an incremental method is more suitable.

The analytical methods are widely used to calculate the stress distribution during the coiling process. The axisymmetric assumption is adopted, and the coiling process is equivalent to the thin-walled cylinders nested layer by layer on a thick-walled cylinder. Using the elastic deformation of the sleeve and coiling tension as boundary conditions, the internal stress of the coil can be calculated by superposition. This method requires the condition that the coil and sleeve are isotropic and have uniform properties at all positions. However, similar to the temperature conduction process, the layered structure of coils can also cause changes in radial mechanical properties, so the radial elastic modulus is normally modified in research [21–23]. Altmann, H.C. [24] considered the anisotropy of coils and established a planar model to solve the stress. In subsequent studies, it was found that the radial elastic modulus was related to interlayer pressure. Hakiel, Z. [25] established a function of radial elastic modulus using radial pressure as a variable to reflect nonlinearity. Based on the model established by Hakiel, Z., Benson, R.C. [26] described the relationship between radial elastic modulus and interlayer pressure using an exponential function. Li, S.P. [27] assumed that the radial elastic modulus was a quadratic function of interlayer pressure and determined the coefficients by laminated compression experiments. For hot-rolled coils, the temperature distribution is not uniform in the radial and axial directions. The above models are limited to the plane assumption and cannot consider the influence of temperature, which may cause certain errors. In order to consider the influence of the temperature field on physical properties, Park, W.W. [28] fitted an axial temperature curve of the strip based on measurements and assumed that each layer of the coil maintained this temperature distribution during the coiling process. In fact, the temperature at different positions of the coil continues to change during the coiling process, which causes changes in physical properties. Therefore, the influence of a dynamic temperature field on stress should be considered.

In summary, the temperature field and stress field during the coiling process interact with each other, and calculating temperature or stress separately may cause certain errors. Meanwhile, due to the real-time changes in temperature and stress state, the incremental model is more in line with the dynamic process. Therefore, a new incremental model for

temperature–stress coupled calculation is established to simulate the coiling process in this article. In order to consider the anisotropy of coils, laminated compression experiments are conducted at different temperatures to obtain the nonlinear relationship between pressure and deformation. Finally, the temperature field results of the model are compared with the measurements to verify the accuracy of the model. The stress field results are compared with the analytical solutions. The differences between the two solutions and the errors caused by analytical methods are analyzed.

2. Materials and Methods

2.1. Establishment of Temperature Field Model

The process of coiling is simplified into thin-walled cylinders nested layer by layer on a thick-walled cylinder. The surface of the coil is covered by a layer of high-temperature strip and forms a new coil. After a period of heat exchange, the new coil is covered by a new layer of high-temperature strip to exchange heat. This process is repeated until the end of coiling, and the heat transfer state of each layer is different and changes in real time during the process. According to the radial heat transfer state, the strips can be divided into two categories: (a) The inner side of the strip is in the contact heat conduction state, while the outer side is in the heat dissipation state exposed to the air; (b) Both the inner and outer sides of the strip are in the contact heat conduction state. The temperature field model is shown in Figure 1. When coiling the $(n + 1)$ layer, the n-th layer is in the heat exchange state (a) and the other layers are in state (b). The duration is the time required to coil the $(n + 1)$ layer. After the coil is covered by the $(n + 1)$ layer, the $(n + 1)$ layer is in state (a) and other layers are in state (b). The duration is the time required to coil the $(n + 2)$ layer. By repeating this process, the temperature distribution at any time during the coiling process can be calculated based on the heat exchange state and time of each layer.

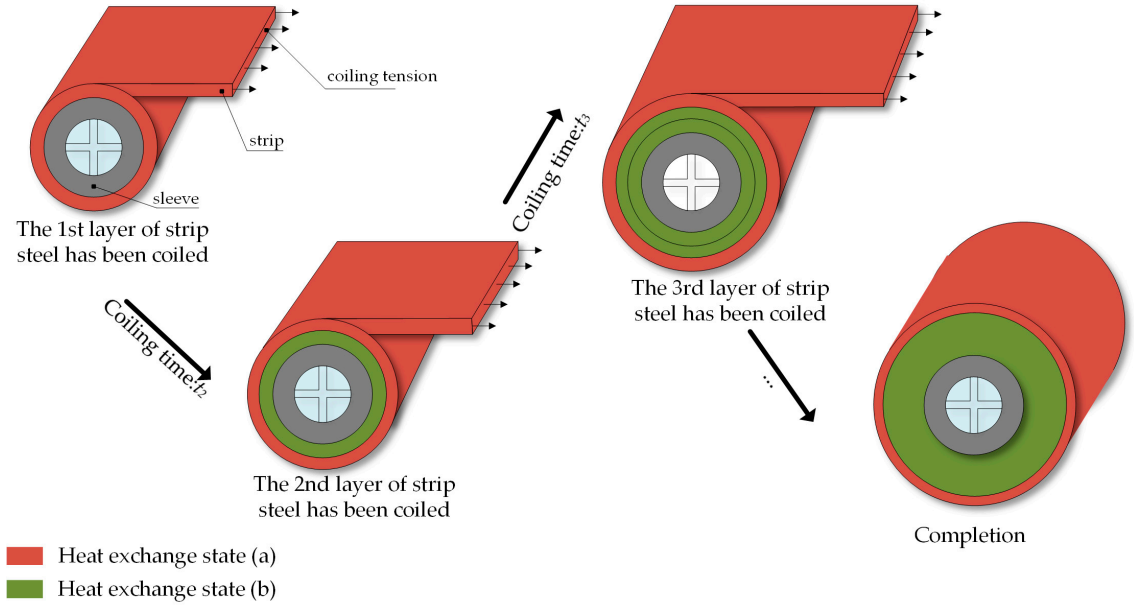

Figure 1. Schematic diagram of heat exchange state of each layer of the coil.

Both the coil and the sleeve can be regarded as axisymmetric thick-walled cylinders, and the thermal conductivity differential equations can be presented as Equation (1).

$$C_p\rho\frac{\partial T}{\partial t} = \lambda_r\left(\frac{\partial^2 T}{\partial r^2} + \frac{1}{r}\frac{\partial T}{\partial r}\right) + \lambda_s\frac{\partial^2 T}{\partial z^2}, \quad (1)$$

where C_p is the specific heat capacity, ρ is the density, T is the temperature, λ_r is the radial thermal conductivity and λ_s is the thermal conductivity of the material itself (for the sleeve, $\lambda_r = \lambda_s$).

To simplify the calculation process, half of the circumferential section of the coil and the sleeve is taken for analysis. Figure 2 shows the circumferential section and the mesh division.

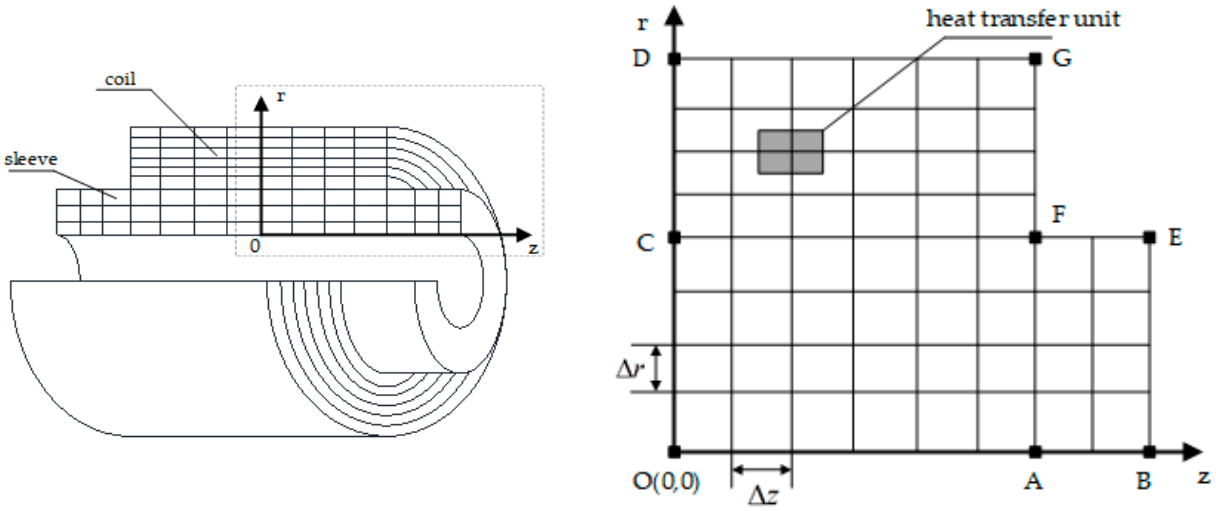

Figure 2. (**a**) Circumferential section of the coil and the sleeve; (**b**) Division of units on the section.

The radial layered structure can be regarded as a continuous superposition of thermal conduction units, as indicated by the shaded areas in Figure 2. The thermal conduction unit is composed of the strip itself, the oxide layer, and the air layer at the contact interface. The thermal resistance of the thermal conduction unit can be presented as Equation (2). The composition of the thermal conduction unit is shown in Figure 3a.

$$R_t = R_s + R_i + R_o, \tag{2}$$

where R_t is the thermal resistance of the thermal conduction unit, and R_s, R_i and R_o are the thermal resistance of the strip, air layer, and oxide layer, respectively.

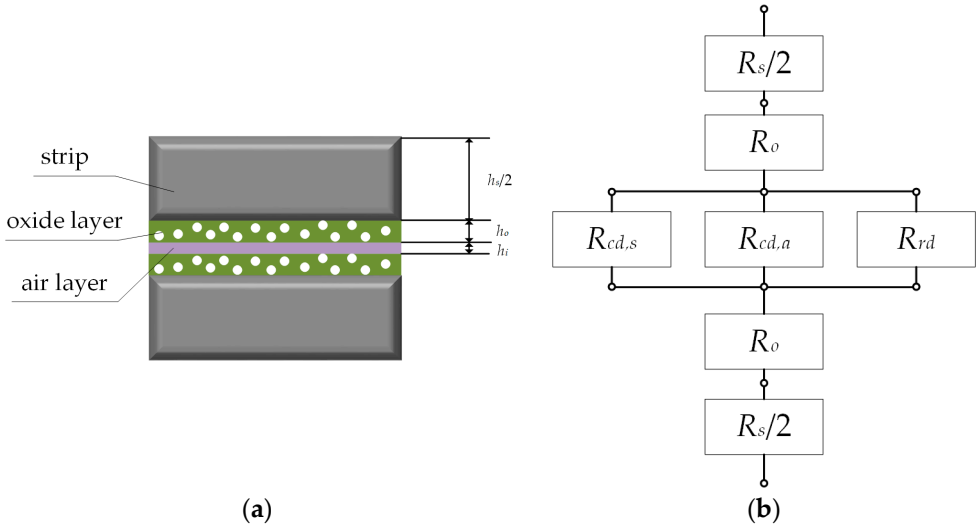

Figure 3. (**a**) Composition of heat transfer unit; (**b**) Thermal resistance of heat transfer unit.

The air layer is the gap left due to insufficient contact between the surfaces of the strips, and there are three ways of heat transfer in the air layer, namely, direct-contact heat transfer on rough surfaces, radiation heat transfer on non-contact parts, and heat transfer of the air in the gap. The total thermal resistance can be calculated as follows:

$$R_i = \frac{1}{\frac{1}{R_{cd,s}} + \frac{1}{R_{rd}} + \frac{1}{R_{cd,a}}}, \tag{3}$$

where $R_{cd,s}$, R_{rd} and $R_{cd,a}$ are contact thermal resistance, radiation thermal resistance, and air layer thermal resistance, respectively, all of which are related to interlayer contact pressure and can be calculated by Equation (4) [29], Equation (5) [15] and Equation (6) [14]:

$$R_{cd,s} = \frac{\sigma_p}{1.13\lambda_s K}\left(\frac{H+P}{P}\right)^{0.94}, \tag{4}$$

$$R_{rd} = \frac{1}{4\left(1-\frac{P}{H+P}\right)\varepsilon \times 5.67 \times 10^{-8} T^3}, \tag{5}$$

$$R_{cd,a} = \frac{42.7 \times 10^{-6} \exp\left(-5 \times 10^{-2} P\right)}{\left(1-\frac{P}{H+P}\right)\lambda_a}, \tag{6}$$

where σ_p is the standard deviation of contour height, K is the absolute value of the average slope of the contour, H is the microhardness, P is the interlayer pressure, λ_a is the thermal conductivity of the air layer and ε is the radiance.

Figure 3b shows the thermal resistance of the thermal conduction unit. By substituting Equations (3)–(6) into Equation (2), the effective thermal conductivity in the radial direction of the coil can be presented as follows:

$$\lambda_r = \frac{\Delta r}{\frac{h_s}{\lambda_s} + 2\frac{h_o}{\lambda_o} + \left[\frac{1}{R_{cd,s}} + \frac{1}{R_{rd}} + \frac{1}{R_{cd,a}}\right]^{-1}}, \tag{7}$$

By substituting the effective thermal conductivity into the thermal conductivity differential equation, the temperature distribution of the coil and sleeve can be obtained. It is worth noting that the effective thermal conductivity is closely related to contact pressure. Therefore, the variation of radial stress distribution inside the coil must be considered during the calculation process.

2.2. Establishment of Stress Field Model

When coiling a layer of strip, it can be regarded as adding a layer of elements on the outer diameter side of the entire grid. The circumferential stress of the new layer of elements is equivalent to the coiling tension. When coiling the $(n + 1)$ layer of strip, material properties and radial elastic modulus can be calculated according to the temperature and interlayer pressure of the first n layers of the coil. After applying the boundary conditions of the outermost tension, the temperature and stress increment can be calculated. By superimposing the increment onto the initial condition, the initial condition for coiling the $(n + 2)$ layer of strip can be obtained. By repeating this process until the end of coiling, the stress distribution of the coil and sleeve can be calculated. Due to the short coiling time, the heat loss of the coil is not significant. The area with a large temperature drop in the coil is relatively small. Compared with the mechanical stress, the thermal stress generated by temperature changes is also relatively small. Therefore, this article mainly focuses on the mechanical stress inside the coil, and the thermal stress is not considered. In addition, the strip hardly slides in the axial and circumferential directions during the coiling process.

Compared to the circumferential stress, the interlayer friction force is smaller and it is not considered in the model. Due to the continuous application of significant coiling tension on the strip in the circumferential direction within a short coiling time, the time–stress relaxation is also not considered. Figure 4 shows the stress distribution inside the coil in the model.

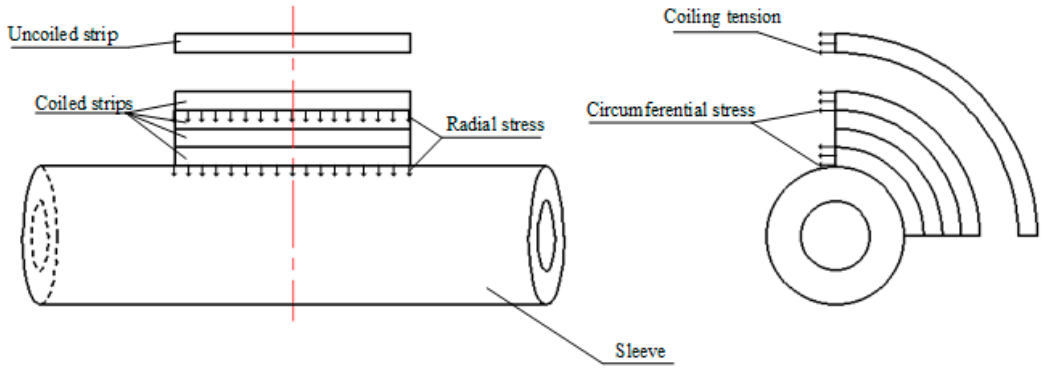

Figure 4. The stress distribution inside the coil in the model.

The completion time of coiling the nth and $(n + 1)$ layer is t_n and t_{n+1}, respectively. In the axisymmetric model, the incremental equilibrium equations for the coil and sleeve can be presented as Equations (8) and (9).

$$\frac{\partial \Delta\sigma_r}{\partial r} + \frac{\partial \Delta\tau_{rz}}{\partial z} + \frac{\Delta\sigma_r - \Delta\sigma_\theta}{r} = 0, \tag{8}$$

$$\frac{\partial \Delta\sigma_z}{\partial z} + \frac{\partial \Delta\tau_{rz}}{\partial r} + \frac{\Delta\tau_{rz}}{r} = 0, \tag{9}$$

where $\Delta\sigma_r$, $\Delta\tau_{rz}$, $\Delta\sigma_\theta$ and $\Delta\sigma_z$ are the increments of radial stress, shear stress, circumferential stress, and axial stress from t_n to t_{n+1}, respectively.

The constitutive equation can be presented as follows:

$$\begin{bmatrix} \triangle\varepsilon_r \\ \triangle\varepsilon_\theta \\ \triangle\varepsilon_z \\ \triangle\gamma_{rz} \end{bmatrix} = \begin{bmatrix} \frac{1}{E^*} & -\frac{\mu}{E} & -\frac{\mu}{E} & 0 \\ -\frac{\mu}{E} & \frac{1}{E} & -\frac{\mu}{E} & 0 \\ -\frac{\mu}{E} & -\frac{\mu}{E} & \frac{1}{E} & 0 \\ 0 & 0 & 0 & \frac{2(1+\mu)}{E} \end{bmatrix} \begin{bmatrix} \triangle\sigma_r \\ \triangle\sigma_\theta \\ \triangle\sigma_z \\ \triangle\tau_{rz} \end{bmatrix} \tag{10}$$

where $\triangle\varepsilon_r$, $\triangle\varepsilon_\theta$, $\triangle\varepsilon_z$, and $\triangle\gamma_{rz}$ are the increments of radial strain, circumferential strain, axial strain, and shear strain of the sleeve unit from t_n to t_{n+1}, respectively, E is the elastic modulus, and E^* is the radial elastic modulus. When the structure is isotropic, $E = E^*$.

By taking strain increment as a known quantity and solving the stress increment in Equation (10), constitutive equations in the sleeve and coil can be obtained.

The sleeve is isotropic, and the incremental constitutive equation can be presented as follows:

$$\begin{bmatrix} \triangle\sigma_r \\ \triangle\sigma_\theta \\ \triangle\sigma_z \\ \triangle\tau_{rz} \end{bmatrix} = \begin{bmatrix} A_1^n & A_2^n & A_2^n & 0 \\ A_2^n & A_1^n & A_2^n & 0 \\ A_2^n & A_2^n & A_1^n & 0 \\ 0 & 0 & 0 & G^n \end{bmatrix} \begin{bmatrix} \triangle\varepsilon_r \\ \triangle\varepsilon_\theta \\ \triangle\varepsilon_z \\ \triangle\gamma_{rz} \end{bmatrix}, \tag{11}$$

where E_t^n is the elastic modulus at t_n. A_1, A_2 and G are the parameters related to elastic modulus and Poisson's ratio, $A_1^n = \frac{(1-\mu_t)E_t^n}{(1-2\mu_t)(1+\mu_t)}$, $A_2^n = \frac{\mu_t E_t^n}{(1-2\mu_t)(1+\mu_t)}$ and $G^n = \frac{E_t^n}{2(1+\mu_t)}$.

The coil is anisotropic and the incremental constitutive equation can be presented as follows:

$$\begin{bmatrix} \triangle\sigma_r \\ \triangle\sigma_\theta \\ \triangle\sigma_z \\ \triangle\tau_{rz} \end{bmatrix} = \begin{bmatrix} B_1^n & B_2^n & B_3^n & 0 \\ B_2^n & B_4^n & B_5^n & 0 \\ B_2^n & B_5^n & B_4^n & 0 \\ 0 & 0 & 0 & G^n \end{bmatrix} \begin{bmatrix} \triangle\varepsilon_r \\ \triangle\varepsilon_\theta \\ \triangle\varepsilon_z \\ \triangle\gamma_{rz} \end{bmatrix}, \quad (12)$$

where E_s^n and E_r^n are the elastic modulus of the strip and the radial elastic modulus of the coil at t_n, respectively. B_1, B_2, B_3, B_4 and B_5 are the parameters related to elastic modulus and Poisson's ratio, $B_1^n = \frac{E_s^n \cdot E_r^n (1-\mu_s)}{E_s^n (1-\mu_s) - 2\mu_s^2 E_r^n}$, $B_2^n = \frac{E_s^n \cdot E_r^n \mu_s}{E_s^n (1-\mu_s) - 2\mu_s^2 E_r^n}$, $B_3^n = \frac{E_s^n \cdot E_r^n (1+\mu_s)}{E_s^n (1-\mu_s) - 2\mu_s^2 E_r^n}$, $B_4 = \frac{(E_s^n)^2 - E_s^n \cdot E_r^n \mu_s^2}{E_s^n (1-\mu_s^2) - 2\mu_s^2 (1+\mu_s) E_r^n}$, and $B_5 = \frac{(E_s^n)^2 + E_s^n \cdot E_r^n \mu_s^2}{E_s^n (1-\mu_s^2) - 2\mu_s^2 (1+\mu_s) E_r^n}$.

When the elastic modulus of the coil is equal in the radial, axial, and circumferential directions, parameter A_1^n is equal to parameter B_1^n and B_4^n, and parameter A_2^n is equal to parameters B_2^n, B_3^n and B_5^n. By substituting the constitutive equation into the equilibrium equation and combining the boundary conditions with the incremental model mentioned above, the internal stress of the coil can be calculated.

Using the temperature and stress at time t_n as initial conditions, the physical properties and thermal parameters can be calculated. The partial differential in the model can be converted into differential form and discretized according to the grid. Then, the equation system can be solved based on the boundary conditions to obtain the temperature increment and stress increment, which can be added to the initial state to obtain the distribution of temperature and stress at time t_{n+1}. The above process is repeated until the end of the coiling process to obtain the distribution of temperature and stress at any time during the coiling process. The numerical calculations are implemented by writing calculation programs in the C programming language. The software used for compilation is Microsoft Visual Studio 2010.

3. Results and Discussion

3.1. Calculation Parameters

According to the actual parameters on the production line, the material of the sleeve is 45 # cast steel and the structure is the four-sided pyramid. The steel grade is Q235B, and the elemental composition is shown in Table 1. Tables 2–4 show the relevant thermal property parameters of the strip, the parameters related to radial thermal conductivity and the parameters of coiling equipment and process in the incremental coupled model, respectively.

Table 1. The elemental composition of materials.

Element	C	Si	Mn	P	S
Content (%)	0.15	0.29	1.2	0.041	0.037

Table 2. Thermal property parameters of the strip.

T (°C)	λ_s (W·m^{-1}·K^{-1})	ρ (kg·m^{-3})	C_p (J·g^{-1}·K^{-1})
30	49.61	7810	0.45
150	47.86	7774	0.50
250	45.45	7742	0.54
350	42.56	7709	0.59
450	39.43	7674	0.65
550	36.41	7638	0.73
650	33.69	7600	0.87

Table 3. The parameters related to radial thermal conductivity, respectively.

h_o (μm)	λ_o (W·m^{-1}·K^{-1})	λ_a (W·m^{-1}·K^{-1})	H (MPa)	σ_p (μm)	K	ε
7	3	0.0048	1133.86	3.22	0.086	0.9

Table 4. The parameters of coiling equipment and process.

Parameters	Value
Thickness h	2.0 mm
Width W	685.0 mm
Coiling speed v	12,700.0 mm/s
Number of layers N	255
Coiling tension σ_T	27.0 MPa
Outer diameter of the sleeve R_m	752.0 mm
Coiling temperature T_s	620.0 °C
Initial temperature of the sleeve T_{t0}	200.0 °C

In order to study the effect of temperature on the elastic modulus of a strip, samples are collected from the site and tensile tests are conducted at the temperature nodes of room temperature, 150 °C, 250 °C, 350 °C, 450 °C, 550 °C, and 650 °C. Figure 5a shows the dimensions of the specimen, and the edges of the specimen are polished. In Figure 5b, the testing machine model is Zwick 150 kN. Figure 5c shows the specimen clamping inside the heating furnace. The temperature inside the heating furnace is raised to the temperature node and held for 60 s. Then, the tensile test is repeated three times at each temperature node and the deformation of the specimen is recorded with an extensometer.

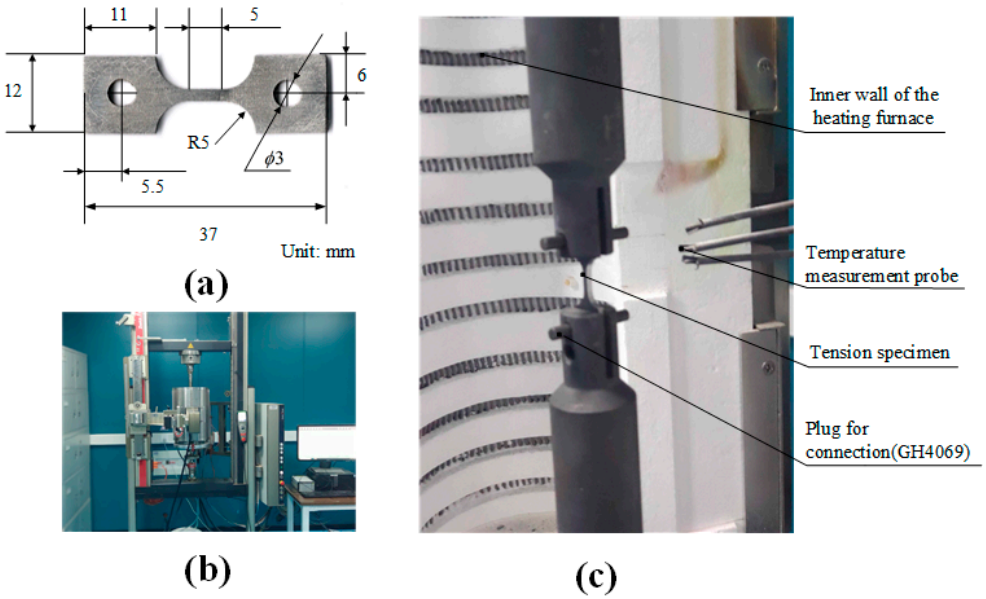

Figure 5. (**a**) Dimension of the tensile specimen; (**b**) Tensile testing machine; (**c**) Clamping of the tensile specimen.

To obtain the radial elastic modulus of the coil, laminated compression experiments are conducted. The strip is cut into circular pieces with a diameter of 20 mm. Each set of the laminates consists of 40 specimens, and compression experiments are conducted at the same temperature node as the tensile tests. The testing machine model is Inspekt Table 100 kN. In order to eliminate the influence of various possible factors such as flatness defects, impurities, and improper operation, each set of the tests is repeated three times. According to the experimental results, the relationship between displacement and pressure

is converted into the relationship between the elastic modulus of the laminated material and the compressive stress.

The trend of elastic modulus variation of a strip is shown in Figure 6a. Figure 6b shows the relationship between the elastic modulus of the laminates and stress at different temperatures. During calculation, the elastic modulus between temperature nodes can be obtained through interpolation.

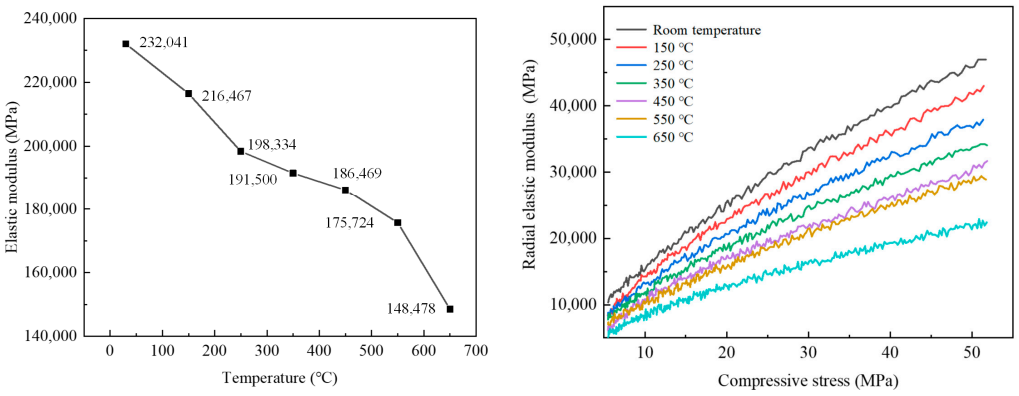

Figure 6. (**a**) Elastic modulus of strip at different temperatures; (**b**) Radial elastic modulus of coil at different temperatures.

3.2. Analysis of Temperature Field Calculation Results

Figure 7 shows the temperature distribution of the circumferential section of the coil and sleeve. From Figure 7a, it can be seen that in the radial direction, because of the heat loss caused by the contact between the coil and the sleeve, there is a significant decrease in temperature near the inner ring of the coil. The number of layers with a temperature drop is 30, with the maximum temperature drop at around 270 °C in the innermost ring. The temperature at the rest positions is close to the coiling temperature. The temperature drop is most significant at the inner ring edges in the axial direction, with a difference of 50 °C from the middle. This is because the heat at the inner ring edges can be transferred along the axial direction of the sleeve. With the increasing of distance from the contact surface, the temperature difference between the edges and the middle decreases by about 18 °C. This is due to the low efficiency and limited time of convective and radiative heat transfer between the axial end faces and the air. The temperature of the sleeve in Figure 7b corresponds to the temperature drop of the coil. There is a severe temperature rise in the contact area, with a maximum value of 180 °C. The thickness of the area where the temperature rises accounts for about 30% of the thickness of the sleeve.

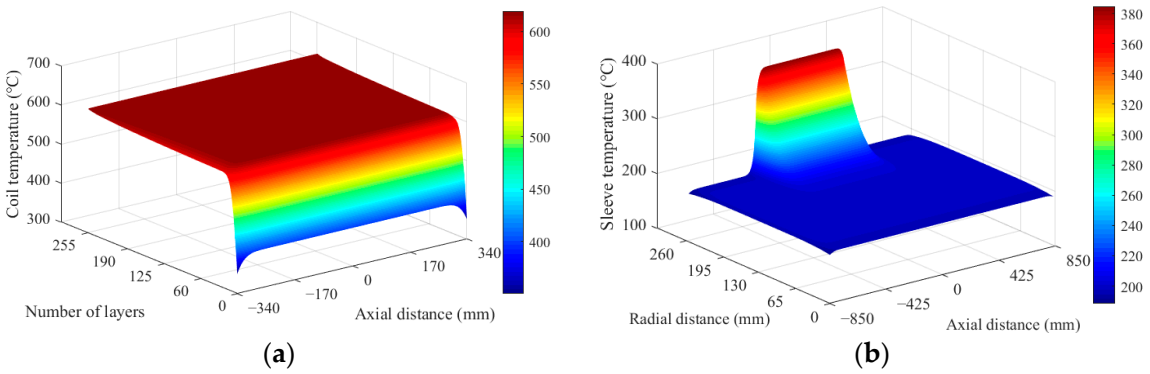

Figure 7. (**a**) Temperature distribution of circumferential section of the coil when the initial temperature of the sleeve is 200 °C; (**b**) Temperature distribution of circumferential section of the sleeve when the initial temperature of the sleeve is 200 °C.

3.3. Analysis of Stress Field Calculation Results

During the coiling process, the radial stress inside the coil is related to the anisotropy, the tightness of the coil and the stress on the sleeve. The circumferential stress and radial stress are interrelated. The coiling tension can be controlled based on the circumferential stress to avoid situations such as loose coiling. Excessive local circumferential stress may cause plastic deformation, resulting in defects in the shape. Therefore, the distribution of radial and circumferential stresses in the coil are mainly discussed. Figure 8 shows the stress distribution of the coil and sleeve after coiling. From Figure 8a, it can be seen that the radial stress is highest at the inner ring and gradually decreases with the increase in radius. The circumferential stress in Figure 8b is relatively high at the inner ring and gradually decreases as it moves away from the contact surface, even transforming into compressive stress near the lowest point. Then, with the increase in radius, the circumferential stress gradually increases to the coiling tension. This distribution pattern is due to the significant difference in radial stiffness between the coil and the sleeve, which limits the radial deformation of the strip. The limit effect is most significant in the innermost ring, resulting in the smallest increment in circumferential compressive stress. When combined with the initial coiling tension, larger circumferential tensile stress is presented. With the increasing of distance from the contact surface, the limit effect gradually weakens and the circumferential compressive stress gradually increases, causing a gradual decrease in circumferential tensile stress. When the compressive stress is larger than the tensile stress provided by the initial coiling tension, the circumferential stress is converted into compressive stress. As the radius increases, the circumferential compressive stress gradually weakens due to the decrease in the number of stacked layers, and the circumferential tensile stress gradually increases to the coiling tension. The difference in the stress of the coil is not significant in the axial direction. This is because the axial temperature difference of the coil is small, resulting in a small difference in mechanical properties.

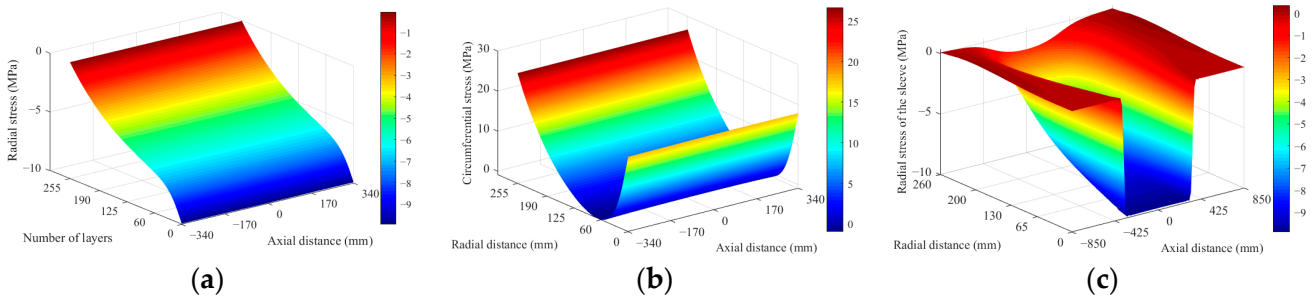

Figure 8. (**a**) Radial stress of the coil; (**b**) Circumferential stress of the coil; (**c**) Radial stress of the sleeve.

3.4. Comparative Analysis of Coupled and Uncoupled Results

During the dynamic coiling process, because of the mutual influence of temperature and stress, the time increment step is reduced and the temperature field and stress field are coupled in the calculation. For the convenience of observing temperature differences, Figure 9 shows the temperature distribution on the axial symmetry plane (OD section in Figure 2). For the coil, the layer range is from 0 to 60 layers, while for the sleeve, the radius range is from R = 260 mm to R = 376 mm.

As shown in Figure 9a, the temperature of the coupled model is relatively high near the contact surface. As the radius increases, both results gradually approach the coiling temperature, but the temperature of the coupled model is smaller. The difference is largest around the 15th layer, about 60 °C. The reason is that the radial stress in the coupled model is relatively high, which increases the radial thermal conductivity. Within the same coiling

time, more heat flows from the coil to the sleeve, resulting in a decrease in temperature of the coil. In Figure 9b, compared with the uncoupled model, the surface temperature rise of the sleeve in the coupled model is larger and the temperature difference is about 50 °C.

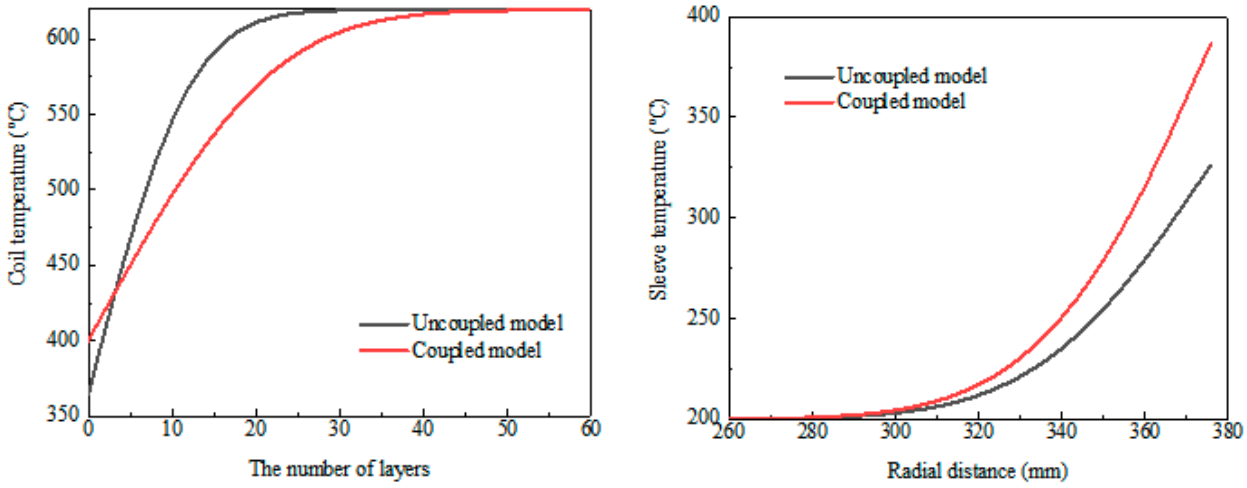

Figure 9. (**a**) Coil temperature; (**b**) Sleeve temperature.

Figure 10 shows the stress comparison between the uncoupled model and the coupled model. The radial stress in the coupled model is relatively large overall. The difference between the two models is largest near the inner ring, about 25%. This is because the influence of temperature on material properties is considered in the coupled model, resulting in a decrease in the elastic modulus. It is more difficult for the sleeve to deform. Corresponding to Figure 10a, circumferential stress of the coupled model in Figure 10b is larger, but the difference between the two models is not significant.

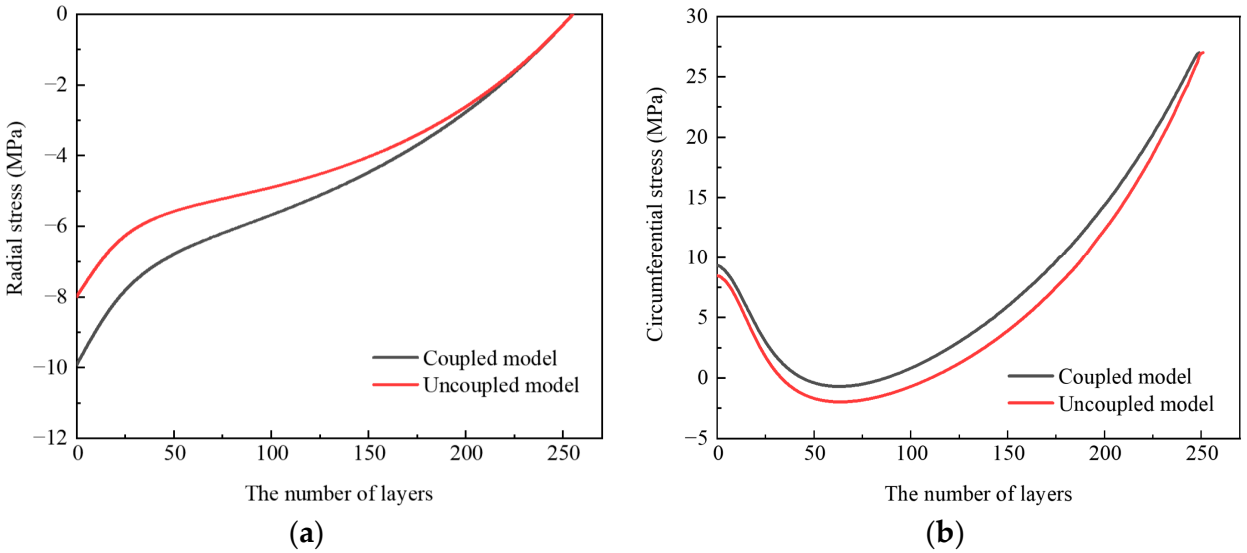

Figure 10. (**a**) Radial stress of the coil in coupled model and uncoupled model; (**b**) Circumferential stress of the coil in coupled model and uncoupled model.

3.5. The Influence of Coiling Process Parameters on Temperature and Stress Distribution

The temperature and stress fields of the coil are affected by the coiling process parameters. Therefore, in this article, the thickness of the strip, the coiling tension, and the initial temperature of the sleeve are taken as variables to study the temperature and stress fields.

Figure 11 shows the calculation results of stress. It can be seen that as the thickness of the strip and the coiling tension increase, and as the initial temperature of the sleeve decreases, the radial stress inside the steel increases. This is because the increase in thickness of the strip and coiling tension both lead to an increase in the total tensile force of the circumferential section, resulting in an increase in the radial stress increment. By reducing the initial temperature of the sleeve, the difference in elastic modulus between the coil and the sleeve is increased. It is more difficult to deform for the sleeve, and the reduction in radial displacement of the coil can lead to an increase in radial stress. In the case of the same radius, the circumferential stress corresponds to the slope of the radial stress curve. This rule is reflected in Figure 11d,f. However, since the horizontal axis represents the number of layers rather than the radius, the rule is not applicable in Figure 11b.

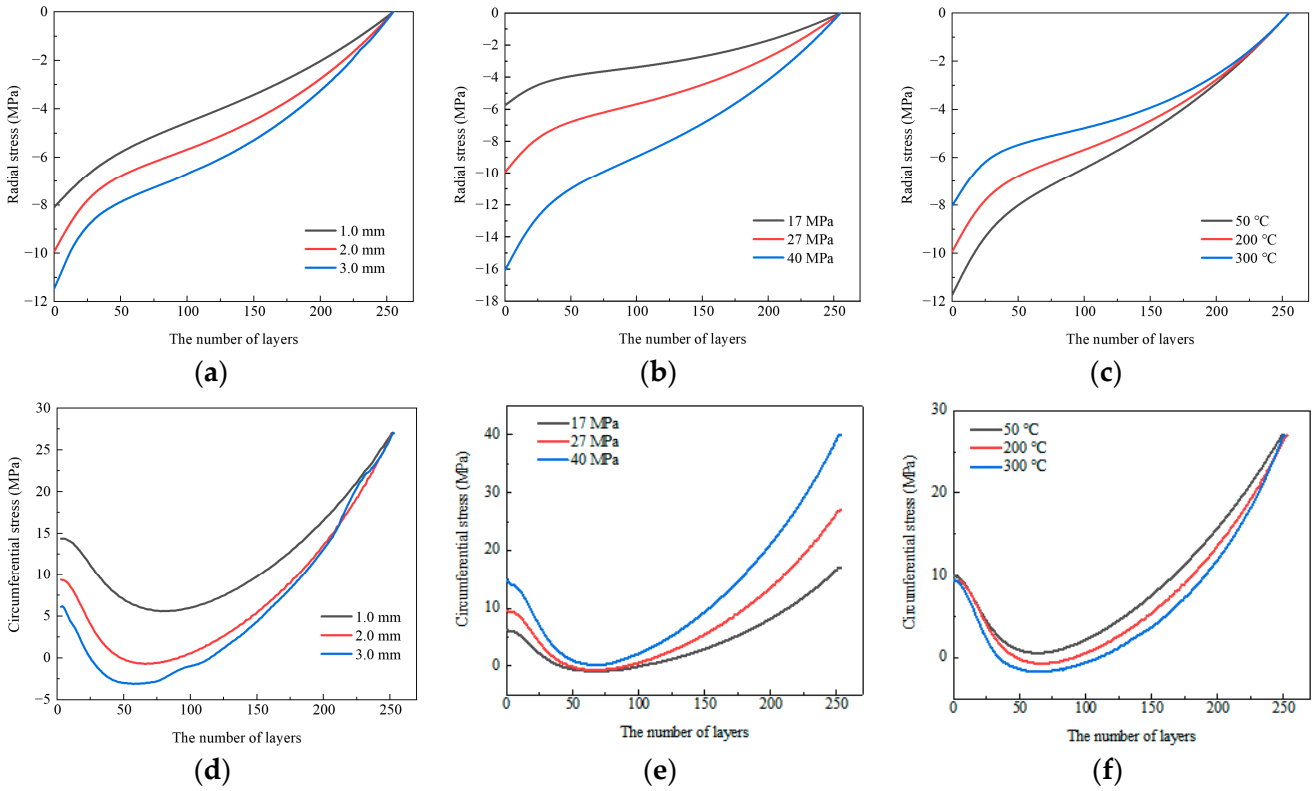

Figure 11. (**a**) The radial stress distribution inside the coil when the thickness of the strip changes; (**b**) The radial stress distribution inside the coil when the coiling tension changes; (**c**) The radial stress distribution inside the coil when the initial temperature of the sleeve changes; (**d**) The circumferential stress distribution inside the coil when the thickness of the strip changes; (**e**) The circumferential stress distribution inside the coil when the coiling tension changes; (**f**) The circumferential stress distribution inside the coil when the initial temperature of the sleeve changes.

Figure 12 shows the temperature calculation results, which indicate that as the thickness of the strip and the coiling tension increase, the temperature rise of the sleeve increases. The reason is that the increase in radial stress leads to an increase in the effective thermal conductivity in the radial direction, causing more heat to flow from the coil to the sleeve, resulting in a corresponding decrease in the temperature of the coil. However, the temperature of the strip of the thickness of 3 mm in Figure 12a is still higher because a thicker strip has a higher total heat content. In Figure 12e, as the initial temperature of the sleeve decreases, the temperature drop of the coil increases. This is because the heat transfer efficiency is improved by the increase in temperature difference on both sides of the contact surface, which is also the reason for the increase in the temperature rise of the sleeve in Figure 12f.

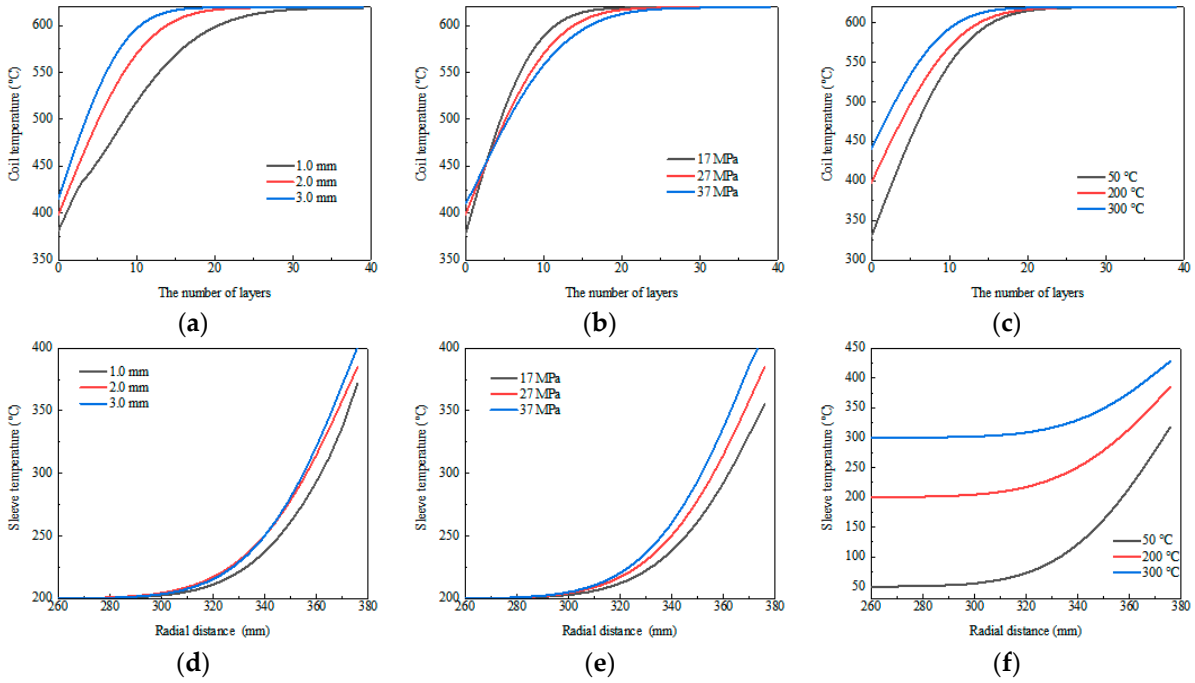

Figure 12. (**a**) Temperature distribution of the coil when the thickness of the strip changes; (**b**) Temperature distribution of the coil when the coiling tension changes; (**c**) Temperature distribution of the coil when the initial temperature of the sleeve changes; (**d**) Temperature distribution of the sleeve when the thickness of the strip changes; (**e**) Temperature distribution of the sleeve when the coiling tension changes; (**f**) Temperature distribution of the sleeve when the initial temperature of the sleeve changes.

3.6. Verification and Analysis of Simulation Results

3.6.1. Comparison Between the Calculated Results and the Measured Temperature

In actual production, due to the direct exposure to air, the temperature of the strip before coiling will be lower than the temperature set by the process and there will be a certain temperature drop at the edges of the strip. Therefore, in this article, the temperature before coiling on the hot-rolling line is measured and the measurement results are fitted. The temperature field is calculated based on the fitting results and compared with measurements on site to verify the correctness of the model. The initial temperature of the sleeve is set to 50 °C, and the other conditions are the same as the parameters in Table 4. Figure 13 shows the temperature distribution of the strip before coiling. The surface temperature of the strip is directly captured by a thermal imaging system, and the model is FLIR-E95.

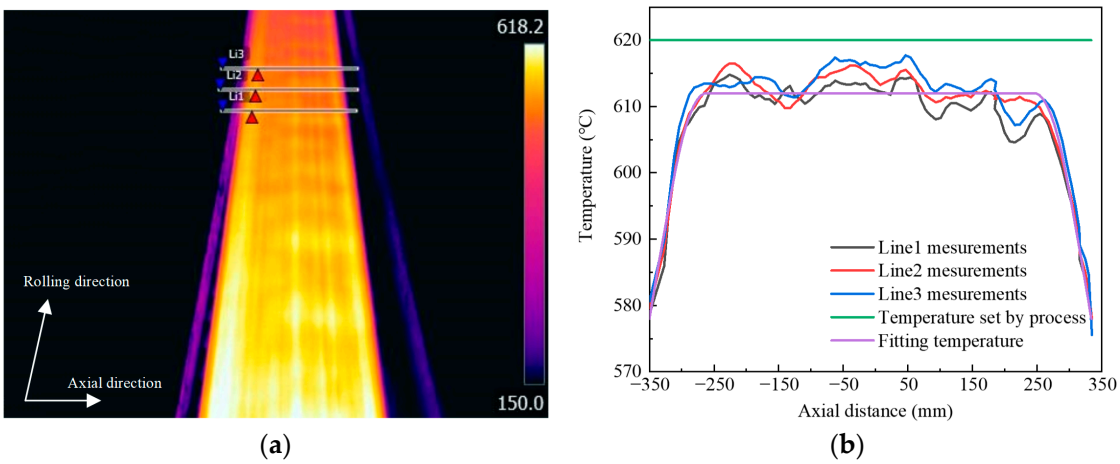

Figure 13. (**a**) Temperature distribution before coiling; (**b**) Measurement results and the fitting curve.

Figure 14 shows the temperature distribution of the circumferential section of the coil and sleeve. Corresponding to the temperature of the strip before coiling, the overall temperature of the coil in Figure 14a is lower than 620 °C and there are obvious low-temperature areas at the edges. The maximum axial temperature difference at the contact surface is about 90 °C. As the position moves away from the contact surface, the temperature difference gradually decreases to the initial temperature difference of 35 °C.

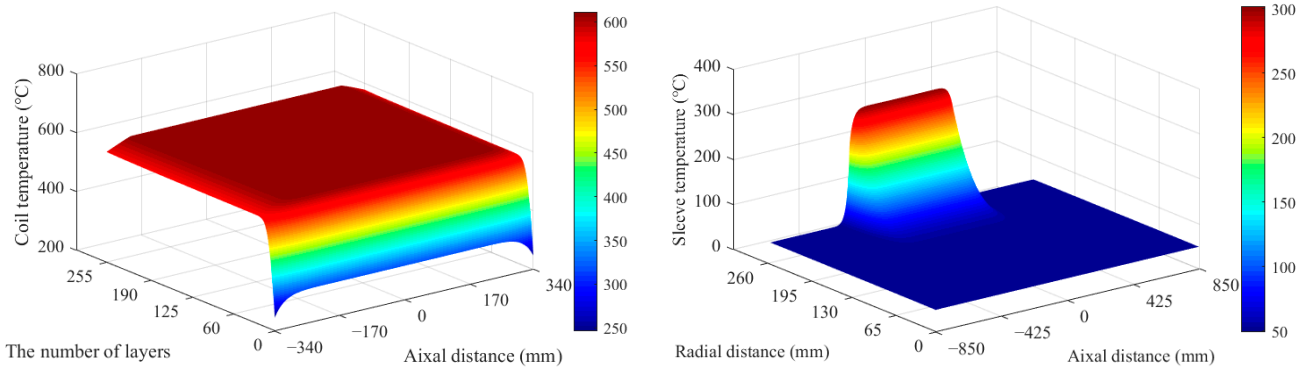

Figure 14. (**a**) Temperature distribution of circumferential section of the coil; (**b**) Temperature distribution of circumferential section of the sleeve.

Due to the difficulty in measuring the internal temperature of the coil, the temperature measurements at the axial end face of the coil and the surface of the sleeve are compared with the calculated results. Figures 15 and 16 are the comparison charts, which show that the calculated results tend to be consistent with the measurements. The error of the surface temperature of the sleeve is less than 30 °C, and the maximum error occurs at the boundary between the contact area and the non-contact area. The reason is that the surface temperature of the sleeve can only be measured after unloading. Due to the heat transfer in the sleeve during the unloading process, the temperature difference between the contact area and the non-contact area is reduced. The maximum temperature error of the coil is less than 20 °C. The above results indicate that the temperature field calculation model established is feasible.

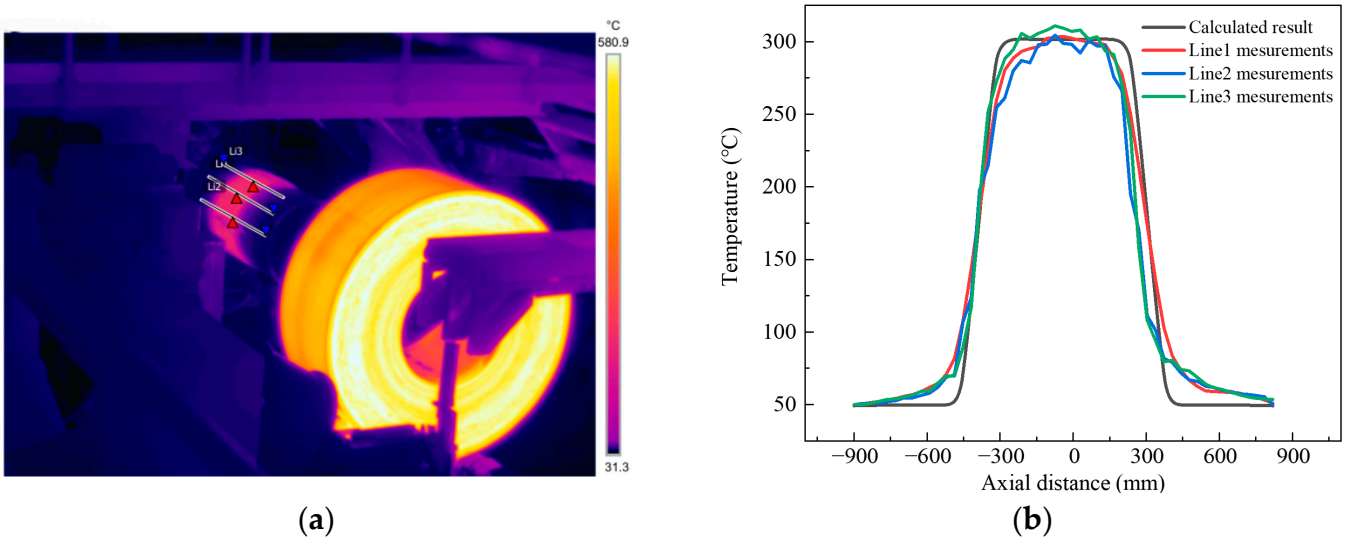

Figure 15. (**a**) The surface of the sleeve after coiling; (**b**) Comparison between calculated result and the measurements.

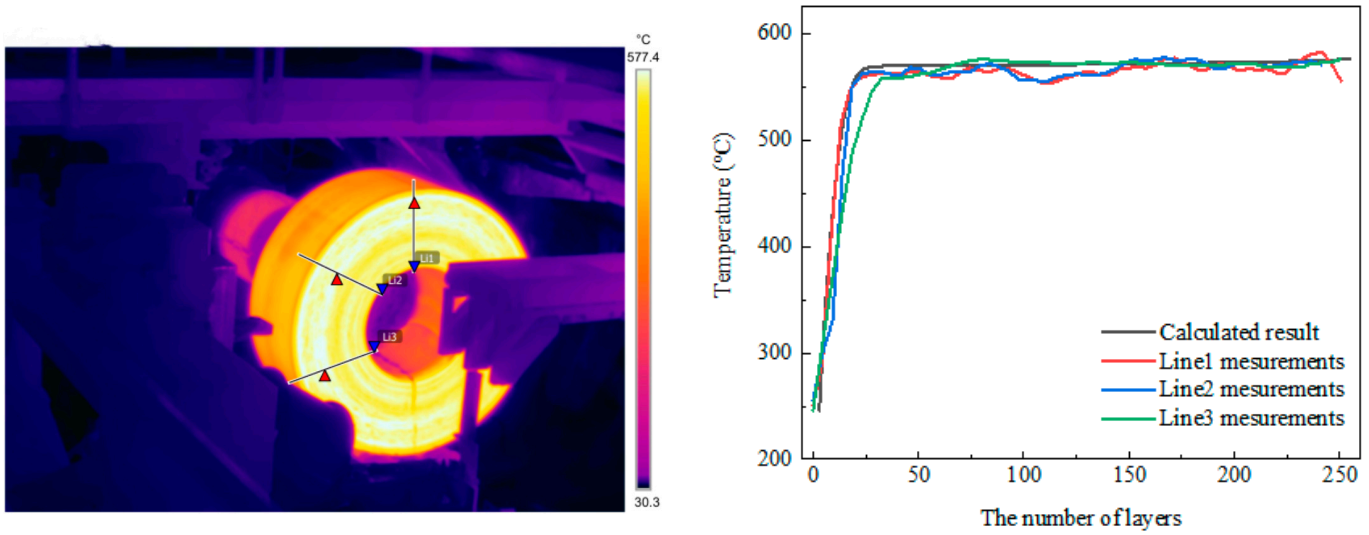

Figure 16. (**a**) The axial end face of the coil after coiling; (**b**) Comparison between calculated result and the measurements.

3.6.2. Comparison of Incremental Coupled Solution and Analytical Solution in Stress

Figure 17 shows the radial and circumferential stress of the coil after coiling. It can be seen that the radial stress near the inner ring is larger in the middle and smaller at the edges in the axial direction. This is because the temperature drop at the edges is relatively large, which leads to the higher elastic modulus and the larger radial displacement at the edges. Corresponding to the radial stress distribution, the circumferential stress in the middle of the coil is larger than that at the edges. In the axial direction, the difference in stress is not significant and gradually disappears with the increase in radius. It is predicted that if the temperature drop at the edges is larger, the stress difference in the axial direction will be more significant.

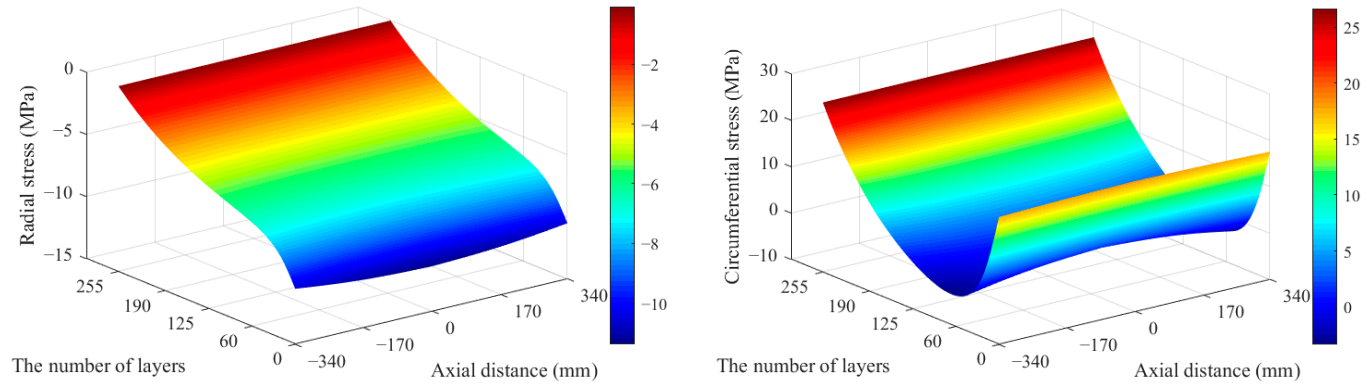

Figure 17. (**a**) Radial stress of the coil; (**b**) Circumferential stress of the coil.

Figure 18 shows the stress difference between the middle and edge of the coil more clearly. During the coiling process, it is very difficult to measure the stress distribution inside the coil. Therefore, it is not possible to prove the validity of the calculated results through experiments. However, analytical methods have been accepted by scholars in academic research and practical production. Therefore, in Figure 18, the analytical solution is compared with the calculated results to verify the rationality, and the differences

between the two methods are analyzed. The analytical solution can be represented by Equations (13) and (14) [30].

$$\sigma_{r,i} = \frac{-\sigma_T \cdot h}{R_i} + \sum_{t=i+1}^{N} \left[\frac{-\sigma_T \cdot h}{R_t} - \frac{\left(\frac{R_t}{R_i}\right)^2 - 1}{\left(\frac{R_t}{R_m}\right)^2 - 1} \cdot \left(p_{1,t} - \frac{\sigma_T \cdot h}{R_t} \right) \right] \tag{13}$$

$$\sigma_{\theta,i} = \sigma_T + \sum_{t=i+1}^{N} \left[\frac{-\sigma_T \cdot h}{R_t} - \frac{\left(\frac{R_t}{R_i}\right)^2 + 1}{\left(\frac{R_t}{R_m}\right)^2 - 1} \cdot \left(p_{1,t} - \frac{\sigma_T \cdot h}{R_t} \right) \right] \tag{14}$$

where $\sigma_{r,i}$ and $\sigma_{\theta,i}$ are radial stress and circumferential stress of the i-th layer and coiling tension. t is the number of coiled layers; R_i and R_t are the radius of the i-th layer and the radius of the coiled layers; $p_{1,t}$ is the contact pressure of the innermost layer when the t-th layer strip has been rolled, which can be obtained from the elastic deformation of the sleeve.

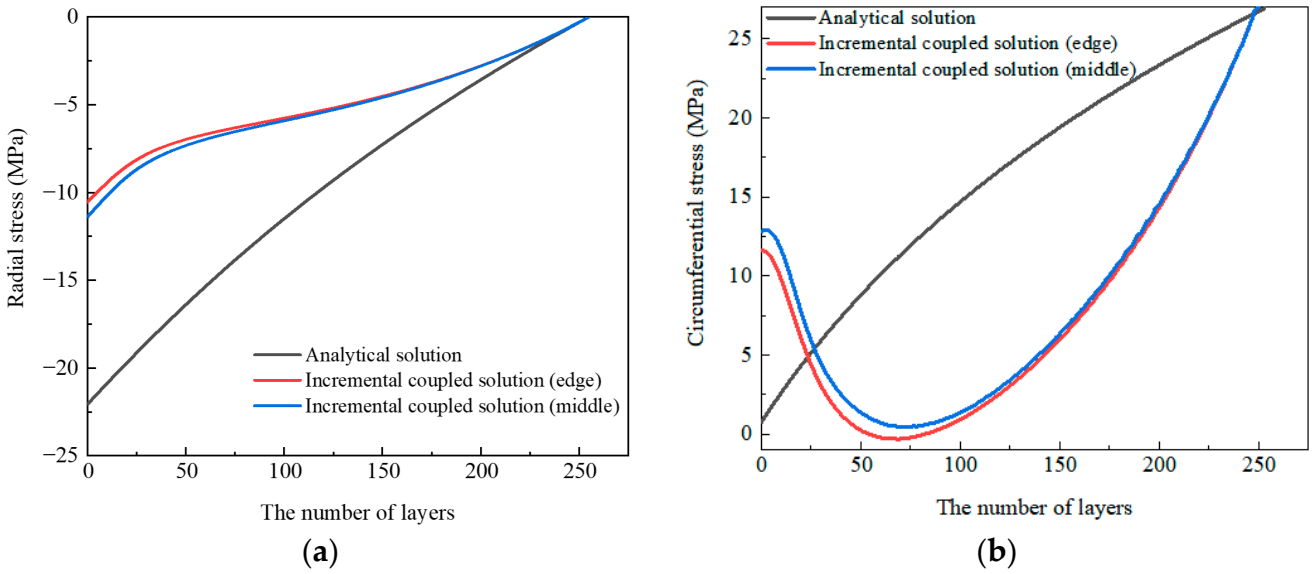

Figure 18. (**a**) Comparison of incremental coupled solution and analytical solution in radial stress; (**b**) Comparison of incremental coupled solution and analytical solution in circumferential stress.

The radial stress trends of the two solutions are the same. But numerically, the incremental coupled solution is relatively small. This is because in the analytical model, the coil and sleeve are considered isotropic. The real-time changes in the radial stiffness caused by interlayer contact and the influence of temperature on the physical properties cannot be considered in the analytical model. According to the comparison, it is safe to design the sleeve and other components based on analytical solutions. However, the temperature results indicate that there is a certain area of temperature rise in the sleeve. If there are defects on the sleeve, such as surface cracks or fatigue damage, the influence of temperature on its physical properties should be considered in the design.

In terms of circumferential stress, the incremental coupled solution is smaller than the analytical solution. This is because the decrease in radial stiffness of the coil in the incremental coupled solution increases the radial deformation of the strip. The circumferential compressive stress increases, and after being added to the coiling tension, the circumferential stress decreases. In the analytical model, if there are enough layers, the circumferential stress near the inner ring may be converted into compressive stress. In fact, because the radial deformation near the inner ring is limited by the sleeve, the circumferential stress remains tensile stress and maintains a certain value. It is worth noting that the

high temperature of the coil leads to a decrease in the yield limit. If the internal stress state is analyzed based on analytical solutions, the plastic deformation generated near the inner ring may be ignored.

4. Conclusions

(1) An incremental calculation model to couple the temperature field and the stress field during the coiling process of hot-rolled strip is proposed. The mutual influence of temperature and stress, the anisotropy of the coil, the uneven axial temperature of the strip and the contact between the coil and sleeve can be considered. The calculation of temperature field and stress field can be closer to actual working conditions.

(2) In production, if the thickness of the strip and the coiling tension are increased and the initial temperature of the sleeve is reduced, the radial stress inside the coil and the surface pressure of the sleeve will be increased to a certain extent. If there are defects such as plastic deformation of the sleeve or the inner layer of the coil, the coiling process can be adjusted according to the above rules. For example, when the strip thickens or the coiling tension increases, the cooling time of the sleeve can be appropriately reduced to increase the initial temperature, thereby reducing the sleeve pressure and internal stress of the coil.

(3) A comparison is made between the incremental coupled solution and the analytical solution. The results indicate that the actual pressure on the sleeve should be much smaller than the analytical solution. Therefore, when the process adjustment increases the pressure, the sleeve designed by the analytical method is safe and can withstand a certain range of increase in pressure. At this point, there is no need to replace the sleeve with a stronger one.

Author Contributions: All authors contributed to the study conception and design. Methodology, H.X. and M.D.; software, Y.H. (Yuting Hu); validation, M.D. and Y.H. (Yanchao Hao); formal analysis, M.D., Y.H. (Yuting Hu) and P.Q.; investigation, M.D. and Y.H. (Yanchao Hao); resources, P.Q.; data curation, Y.H. (Yuting Hu); writing—original draft preparation, M.D.; writing—review and editing, P.Q., H.X. and M.D.; visualization, Y.H. (Yanchao Hao); supervision, H.X.; project administration, H.X.; funding acquisition, H.X. All authors have read and agreed to the published version of the manuscript.

Funding: This work was supported by the National Natural Science Foundation of China (Funder: Hong Xiao and the funding number: 51474190).

Data Availability Statement: The data presented in this study are available on request from the corresponding author due to privacy.

Acknowledgments: The authors would like to thank the National Engineering Research Center for Equipment and Technology of Cold Rolled Strip in Yanshan University for assistance in the tests.

Conflicts of Interest: The authors declare no conflicts of interest.

References

1. Zhou, C.; Le, Q.C.; Wang, T.; Liao, Q.Y.; Zhu, Y.T.; Zhao, D.Z.; Bao, L.; Jia, W.X. Effect of asymmetry on microstructure and mechanical behavior of as-rolled AZ31 magnesium alloy medium plates during coiling at warm temperatures. *Mater. Sci. Eng. A.* **2024**, *894*, 146474. [CrossRef]
2. Wang, C.; Wu, H.B.; Zhang, Y.Y. Structural transformation behavior of oxide scale during coiling of 0.9 wt% Cr-containing high-strength steel. *J. Mater. Res. Technol.* **2024**, *30*, 840–853. [CrossRef]
3. Dai, M.; Liang, S.J.; Qiu, P.; Xiao, H. Simulation of cold rolling strip coiling process considering additional contact deformation. *Iron Steel* **2023**, *58*, 80–86.
4. Gu, C.; Scott, C.; Fazeli, F.; Gaudet, M.J.; Su, J.; Wang, X.; Bassim, N.; Zurob, H. Evolution of the microstructure and mechanical properties of a V-containing microalloyed steel during coiling. *Mater. Sci. Eng. A* **2023**, *880*, 145332. [CrossRef]
5. Gu, C.; Scott, C.; Fazeli, F.; Wang, X.; Bassim, N.; Zurob, H. Site-specific analysis of precipitates during the coiling of an HSLA steel containing V and Nb. *J. Mater. Res. Technol.* **2023**, *27*, 6308–6318. [CrossRef]
6. Chen, D.M.; An, Z.Z.; Wang, G.D.; Liu, T.H. Effects of hot rolling and coiling temperatures on microstructure, texture and magnetic properties of 1.6 wt% Si non-oriented silicon steel. *Mater. Today Commun.* **2022**, *31*, 103807. [CrossRef]

7. Xiao, B.; Yu, Y.S.; Hu, B.; Wang, H.R.; Wang, W.; Liu, S.L.; Misra, R.D.; Liu, W.Q. On balanced strength and ductility synergy in low alloy steels through multiphase heterostructure involving cumulative process of hot rolling, coiling and tempering. *Mater. Sci. Eng. A* **2024**, *891*, 145987. [CrossRef]
8. Wu, H.; Sun, J.; Peng, W.; Jin, L.; Zhang, D.H. A symplectic analytical approach for thermal-metallurgical coupling problems: A case study of hot-rolled coil cooling. *Int. J. Heat Mass Transfer.* **2024**, *223*, 125218. [CrossRef]
9. Wang, X.D.; Wang, Z.Y.; Tang, W.; Li, J.; Liu, B.; Bai, H.K. Study on heart shaped buckling mechanism and prevention method of thin silicon steel. *J. Mech. Eng.* **2023**, *59*, 123–131.
10. Dai, M.; Liang, S.J.; Qiu, P.; Xiao, H. Efficient finite element simulation of cold rolled strip coiling process considering additional contact deformation between layers. *ISIJ Int.* **2024**, *64*, 1037–1046. [CrossRef]
11. Yang, L.Z.; Du, S.H.; He, F.M.; Zhang, Z.J. Three-dimensional thermoelastic analysis of orthotropic laminated cylindrical shells subjected to uniformly localized thermal boundary conditions. *J. Therm. Stresses* **2023**, *46*, 1227–1247. [CrossRef]
12. Nam, A.; Prüfert, U.; Pietrzyk, M.; Kawalla, R. Coil model for magnesium alloy strips and its heat transfer analysis. *Procedia Manuf.* **2018**, *15*, 185–192. [CrossRef]
13. Mats, K. Modelling of the temperature distribution of coiled hot strip products. *ISIJ Int.* **2011**, *51*, 416–422.
14. Baik, S.C.; Kwon, O.; Park, S.J.; Hong, B.H.; Oh, K.H. Analysis of heat transfer in hot rolled coils for optimum condition of forced cooling. *Met. Mater.* **1999**, *5*, 369–375. [CrossRef]
15. Park, S.J.; Hong, B.H.; Baik, S.C.; Oh, K.H. Finite element analysis of hot rolled coil cooling. *ISIJ Int.* **1998**, *38*, 1262–1269. [CrossRef]
16. Jung, Y.J.; Lee, G.T.; Kang, C.G. Coupled thermal deformation analysis considering strip tension and with/without strip crown in coiling process of cold rolled strip. *J. Mater. Process. Technol.* **2002**, *130–131*, 195–201. [CrossRef]
17. Saboonchi, A.; Hassanpour, S. Heat transfer analysis of hot-rolled coils in multi-stack storing. *J. Mater. Process. Technol.* **2007**, *182*, 101–106. [CrossRef]
18. Saboonchi, A.; Hassanpour, S. Simulation-based prediction of hot-rolled coil forced cooling. *Appl. Therm. Eng.* **2008**, *28*, 1630–1637. [CrossRef]
19. Cheng, J.F.; Liu, Z.D.; Dong, H.; Gan, Y. Analysis of the factors affecting thermal evolution of hot rolled steel during coil cooling. *J. Univ. Sci. Technol. Beijing* **2006**, *13*, 139–143. [CrossRef]
20. Witek, S.; Milenin, A. Numerical analysis of temperature and residual stresses in hot-rolled steel strip during cooling in coils. *Arch. Civ. Mech. Eng.* **2018**, *48*, 659–668. [CrossRef]
21. Liu, M.L. A nonlinear model of center-wound rolls incorporating refined boundary conditions. *Comput. Struct.* **2009**, *87*, 552–563. [CrossRef]
22. Wang, Y.Q.; Li, L.; Yan, X.C.; Luo, Y.X.; Wu, L. Modeling of stress distribution during strip coiling process. *J. Iron Steel Res. Int.* **2012**, *19*, 6–11. [CrossRef]
23. Xiao, H.; Xu, Z.A.; Zhang, C.J. Incremental solution of internal stress incoiling process of cold rolled strip. *Iron Steel* **2020**, *55*, 82–87.
24. Altmann, H.C. Formulas for computing the stresses in center-wound rolls. *Tappi J.* **1968**, *51*, 176–179.
25. Hakiel, Z. Nonlinear model for wound roll stresses. *Tappi J.* **1987**, *70*, 113–117.
26. Benson, R.C. A nonlinear wound roll model allowing for large deformation. *J. Appl. Mech.* **1995**, *62*, 853–859. [CrossRef]
27. Li, S.P.; Cao, J. A hybrid approach for quantifying the winding process and material effects on sheet coil deformation. *Eng. Mater. Technol.* **2004**, *126*, 303–313. [CrossRef]
28. Park, W.W.; Kim, D.K.; Im, Y.T.; Kwon, H.C.; Chun, M.S. Effects of processing parameters on elastic deformation of the coil during the thin-strip coiling process. *Met. Mater. Int.* **2014**, *4*, 719–726. [CrossRef]
29. Mikić, B.B. Thermal contact conductance: Theoretical considerations. *Int. J. Heat Mass Transfer.* **1974**, *17*, 205–214. [CrossRef]
30. Doghri, I. *Mechanics of Deformable Solids: Linear and Nonlinear Analytical and Computational Aspects*, 1st ed.; Springer: Berlin/Heidelberg, Germany, 2000; pp. 193–232.